Cosmic Ray Composition from the 40-string IceCube/IceTop Detectors

THE ICECUBE COLLABORATION[1]

[1] *See special section in these proceedings*

Abstract: The IceCube Observatory at the South Pole is composed of a deep detector and a surface detector, IceTop, both of which use Cherenkov light to detect charged particles. Cosmic ray air showers contain multiple particle components: in particular, electrons and muons detectable at the surface by IceTop, and high-energy muons detectable by the deep IceCube detector, in relative amounts that depend on the primary cosmic ray mass. Thus, coincident events can be used to measure both the energy and the mass composition. Here, a neural network is trained with simulations to map observables from the two detectors (input) into energy and mass estimators (output). Experimental data is then run through the same network, to measure the energy spectrum and average logarithmic mass of cosmic rays in the energy range of about 1-30 PeV.

Corresponding authors: K. Andeen[2] (*karen.andeen@icecube.wisc.edu*), K. Rawlins[3], T. Feusels[4]

[2]*Dept. of Physics, University of Wisconsin-Madison, WI 53706, USA (now at Rutgers University)*
[3]*Dept. of Physics and Astronomy, University of Alaska Anchorage, AK 99508, USA*
[4]*Dept. of Physics and Astronomy, Gent University, B-9000 Gent, Belgium*

Keywords: mass; composition; knee; IceCube; IceTop

1 Introduction

Measuring more than one particle component of a cosmic ray air shower is a powerful tool for separating light and heavy nuclei in Extensive Air Shower (EAS) data, at energies at the knee and above where direct measurements of cosmic rays are not possible. The IceCube Observatory at the South Pole is being used in such a manner, with an array of light sensors (Digital Optical Modules, or DOMs) buried on strings between 1450 and 2450 m (herein "Ice-Cube") together in coincidence with a corresponding array of DOMs in frozen water tanks on the surface ("IceTop"). An IceTop "station" is two tanks separated by 10 m; Ice-Cube strings and IceTop stations are separated by 125 m [1].

Both instruments measure the Cherenkov light emitted by charged particles through the surrounding medium. In Ice-Top, the medium is water frozen in tanks at the site. The DOMs in the tanks measure light from the electromagnetic and GeV muonic components of the EAS. In IceCube, the medium is the Antarctic icecap, and the deeply-buried DOMs measure light from high-energy (TeV) muons bundled near the central axis of the shower.

2 Reconstruction

Events in IceTop are reconstructed by a likelihood method [3], comparing the detected signal locations, charges, and times from hit stations (as well as the locations of not-hit stations) to what is expected from a cosmic ray EAS. Signal *times* are compared to an expected timing profile, and signal *charges* are compared to an expected lateral distribution function (LDF). The LDF used, a function of the perpendicular distance from the shower axis, r, is known as the "Double Logarithmic Parabola,":

$$S(r) = S_{\text{ref}} \cdot \left(\frac{r}{R_{\text{ref}}} \right)^{-\beta - \kappa \log_{10}\left(\frac{r}{R_{\text{ref}}} \right)}. \qquad (1)$$

The logarithm of the signals S are assumed to have normal distributions, and are expressed in units of "vertical equivalent muons" (VEM). Here, R_{ref} represents a "reference distance" from the shower axis, and S_{ref} is the signal strength at that reference distance. The reference distance found to have the most robust measurement at these energies is 125 m [3], so S_{125} is the observable representing the "shower size".

Events in IceCube are reconstructed with a similar philosophy: the signals N_{PE}, measured in photoelectrons, are compared to an LDF which is a function of perpendicular

distance to the track d (described in detail in [4, 5, 6]):

$$N_{PE}(d, X, z) = A \left[\frac{a}{b} \left(e^{bX} - 1 \right) \right]^{-\gamma_\mu} \frac{e^{-d/(c_{ice}(z) \cdot \lambda_0)}}{\sqrt{(c_{ice}(z) \cdot \lambda_0) d}}.$$
(2)

This function of d is dominated by the decaying exponential; the "slope" of this exponential is the attenuation length of light in the ice. Since the clarity of the ice changes due to well-measured horizontal dust layers [7, 8], this slope is treated as a bulk attenuation length λ_0 multiplied by a depth-dependent correction factor c_{ice} based on scattering length data measured at different depths z. The first term, containing the slant depth from the snow surface X, corrects for the ranging-out of muons as they penetrate deeper into the ice; the parameters a, b, and γ_μ in the first term are constants.

The overall normalization of this LDF scales with the energy deposited by muons in the detector, and this is parametrized with K_{70}, which is the expected signal (given by Equation (2)) evaluated using reference values of X = 1950 m, $c_{ice} = 1$, and at a perpendicular distance $d =$ 70 m. Since the track direction affects the signal expectation N_{PE} at all the DOMs (by changing d and X), the same likelihood function can also be used to find the track direction. These two reconstruction techniques (using surface signals to find the core position and S_{125} in IceTop, and using signals in IceCube to find the track direction and K_{70}) are used iteratively to find a reliable best-fit track.

3 Data, Simulation, and Event Selection

This analysis used data from August 2008, when the detector was in its 40-string/40-station configuration, for an overall detector livetime of 29.78 days. Because of unsimulated effects near the detector threshold due to snow buildup over tanks deployed before 2007, data from the subarray of IceTop deployed after 2007 were used. Monte Carlo simulated events were produced using the CORSIKA air shower generator [9] with the SIBYLL-2.1/FLUKA-2008 hadronic interaction models [10, 11], and an atmospheric model representing austral winter at the South Pole. Five particle species (proton, helium, oxygen, silicon, and iron) were generated according to an E^{-1} spectrum from 1 TeV to 46.4 PeV. The showers (3000 of them per species per third of a decade in energy) were generated uniformly over all azimuths and to a zenith angle of 65°, oversampled 100 times, and thrown over a circle of radius 1200 m centered on IceTop. The response of the IceTop tanks, the propagation of the high-energy muons through the ice to the depth of IceCube, the Cherenkov photons propagating to the DOMs, and the response of the DOMs themselves, are included in a detector simulation.

Quality cuts were applied to select those events which were well-reconstructed and contained within both the IceTop area and IceCube detector volume. Parameters such as track length and reconstructed effective propagation length (λ_0) were used to quantify reconstruction quality (see [6]

for details). These cuts allow for a resolution (containing 68% of events) of better than 9 m in core position and less than 0.5° in track direction. The final event sample contains 239797 events from the August 2008 experimental data and 20289 total simulated events of five primary species.

4 Neural Network Mapping Technique

Once S_{125} and K_{70} have been reconstructed and quality cuts applied, simulations show that light and heavy nuclei are separated in this two-dimensional parameter space, as shown in Figure 1. The relation between the K_{70}-S_{125} space and the mass-energy space is non-linear, therefore a mapping technique is required to correlate one space to the other.
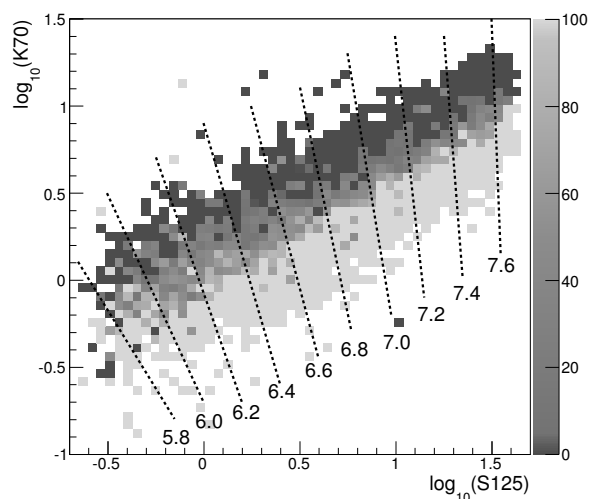

Figure 1: Fraction of each bin populated by protons (when only protons and iron are included in the sample). Dark grey indicates 100% iron, light grey indicates 100% protons; intermediate greys indicate overlapping populations. The dotted black lines approximating energy contours guide the eye for both nuclei.

A neural network was chosen for this work, which consists of a set of input parameters (in this case, K_{70} and S_{125}) which are connected to a set of output parameters (in this case, $\log_{10}(E)$ and $\ln(A)$) through a series of nodes which are arranged in layers. Each node is connected to other nodes in the previous and subsequent layer via a series of weights. At each node, an activation function acts on its input parameters as modified by the weights. Both the two inputs and the two outputs are renormalized so that they are numbers between zero and one.

The weights relating the inputs to the outputs are determined by "training" the network on a subsample of the Monte Carlo simulations (1/4 of the events) for which the true energy and true mass are known. Through a series of learning cycles, the network adjusts the weights to improve the accuracy of reconstructed outputs. A "testing" sample

(an independent 1/4 of the events) are put through the network after each learning cycle and the errors monitored to ensure that the network is not becoming too specific to the training events, or being "overtrained". The remaining half of the simulated data is known as the "analysis" sample and was used for the final steps described in section 6 below.

5 Energy Spectrum

For each event of experimental data, the neural network assigns a reconstructed energy and a reconstructed mass parameter. Reconstructed energies agree well with the true energies of simulated events; Figure 2 shows the energy resolution, and the reconstruction bias, as a function of energy.
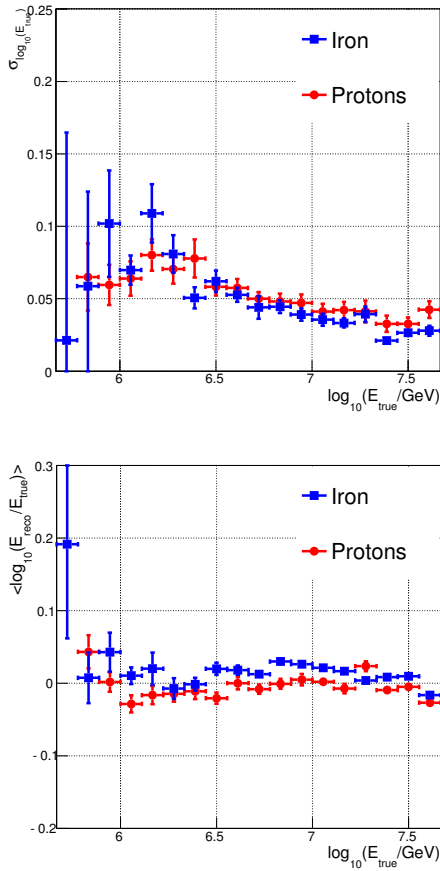

Figure 2: Upper: The energy resolution of the neural network output (sigma of distribution of $\log(E_{reco}) - \log(E_{true})$). Lower: The bias or misreconstruction of energy (mean of that distribution).

From these reconstructed energies, one can create an all-particle energy spectrum from experimental data. For a given flux Ψ as a function of energy E_0,

$$\Psi(E_0) = \frac{1}{\eta A \Omega \tau} \frac{dN}{dE} = \frac{1}{\eta A \Omega \tau} \frac{0.4343}{E_0} \frac{dN}{d\log_{10}(E_0)}, \quad (3)$$

where η is the efficiency (the ratio of simulated events left after all cuts to the number generated, which is a function of E_0), A is the area over which the CORSIKA showers were thrown, τ is the livetime of the detector (in this case 29.78 days), and Ω is the solid angle over which the events were generated. The resulting energy spectrum is shown in Figure 3.
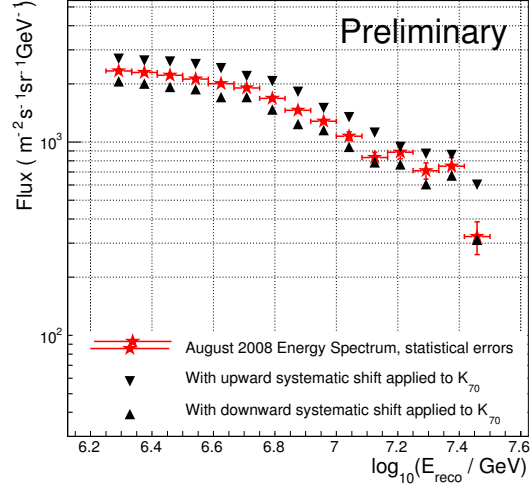

Figure 3: Measured all-particle flux as a function of particle energy, from August 2008 experimental data, with statistical error bars. Triangles indicate alternate spectra derived from data with K70's shifted up or down by 22.2% (see section 7).

6 Mass Composition

Within each slice in energy and for each simulated species, the neural network produces a distribution of mass outputs which is called a "template histogram". Examples of template histograms for three kinds of primaries are shown in Figure 4, for one slice in energy as an example. Data, when put through the same neural network, also has a histogram of outputs which can be decomposed into a linear combination of the template histograms of the individual species (proton, oxygen, etc.). A minimizer finds the optimal mixture of simulated species to match the data.

Proton and iron template histograms alone are not sufficient to reproduce the data, and so intermediate nuclei are necessary. Because there is a great deal of overlap between the template histograms of all five nuclei, we matched the data to a combination of three template histograms: protons, iron, and "intermediate nuclei" (which is a 50-50 mixture of helium and oxygen). When this procedure is applied to a "hand-mixed" sample of Monte Carlo events (treating the sample like data, with different $\ln(A)$ at different energies), the fit found mixtures which correctly reproduced the $\ln(A)$ at all energies. When the procedure was applied to
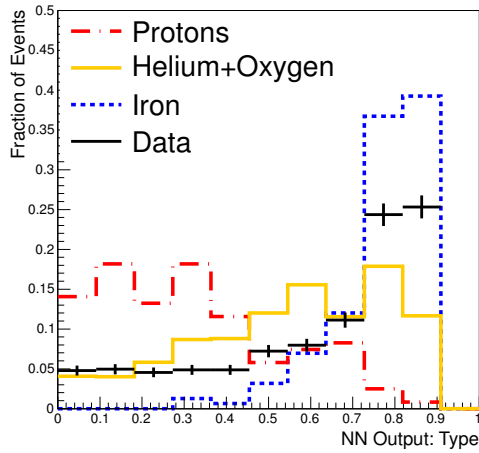
Figure 4: Three "template histograms": protons, iron, and a 50-50 mixture of helium and oxygen. The energy bin shown here is $\log_{10}(E/\mathrm{GeV})$ from 6.9 to 7.1.

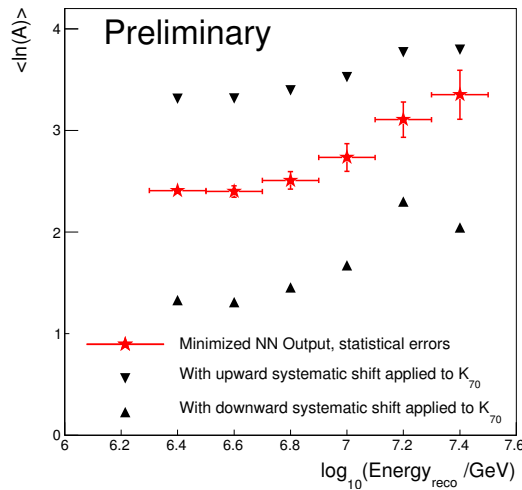experimental data from August 2008, the $\ln(A)$ as a function of energy was computed and is shown in Figure 5.

Figure 5: Measured $\ln(A)$ as a function of reconstructed energy, with statistical error bars. Triangles indicate alternate results if K70 is shifted up or down by 22.2%.

7 Systematic Errors

Both Figures 3 and 5 include estimates of the systematic error due to a variety of effects:

- *Hadronic Interaction Model:* Samples of events simulated with both EPOS-1.99 [12] and QGSJET-II-03 [13] were generated for comparison with SIBYLL. *Percent error in K_{70}: 9.7%*

- *Ice Model:* Since K_{70} depends on the propagation of photons through the ice, the effect of two different models of the attenuation of light in dust layers (known as AHA [7] and SPICE [8]) were investigated. *Percent error in K_{70}: 9.7%*

- *DOM Efficiency:* The efficiency of the DOMs in IceCube depends upon a number of factors, which have been measured in a controlled setting [14]. *Percent error in K_{70}: 8%*

- *Errors introduced from corrections:* The Monte Carlo simulation used for this work did not include two relevant effects: a recent improvement of the parameterization of the light yield from muon bundles in IceCube, and the accumulation of snow on the surface above IceTop. The effects were quantified and corrected for, but some error due to the application of this correction was estimated. *Percent error in K_{70}: 14.8% and 4.7%, respectively*

The total systematic shift in K_{70} (added in quadrature) is 22.2%. The effect of these systematics on the final results (i.e. the spectrum in Figure 3 and the mass composition in Figure 5) were studied by applying these errors as shifts to the input parameters of the neural network (i.e. K_{70}) before it goes through the neural network, and seeing how the output parameters, and any analysis downstream of the neural network, changes. Both of these figures show alternative results with such a shift (both up and down) applied. If improved simulations eliminate the errors introduced from corrections, the total systematic error could be substantially reduced.

References

[1] H. Kolanoski, IceCube summary talk, these proceedings.

[2] The IceCube Collaboration, paper 807, these proceedings.

[3] S. Klepser, PhD thesis, Humboldt Univ, Berlin (2008)

[4] K. Rawlins, PhD thesis, Univ. of Wisconsin-Madison (2001)

[5] J. Ahrens et al., *Astropart. Phys.* **21** (2004) 565-581.

[6] K. Andeen, PhD thesis, Univ. of Wisconsin-Madison (2011)

[7] M. Ackermann et al., *J. Geophys. Res.*, **11** (2006)

[8] "Study of South Pole ice transparency with IceCube flashers" (The IceCube Collaboration), to be published.

[9] D. Heck, et al., *Forschungszentrum Karlsruhe Report FZKA 6019* (1998)

[10] E. J. Ahn et al. *Phys. Rev. D* **80** (2009) 94003.

[11] G. Battistoni et al., *AIP Conf. Proc.*, **896** (2007) 31.

[12] K. Werner *Nucl. Phys. B Proc. Suppl.*, **175** (2007) 81.

[13] N. N. Kalmykov, S. S. Ostapchenko and A.I. Pavlov, *Nucl. Phys. B Proc. Suppl.*, **52** (1997) 17.

[14] R Abbasi et al., *Nucl. Inst. and Methods in Phys. Res. Section A*, **618** (2010) 139.